TALLINN UNIVERSITY OF TECHNOLOGY
SCHOOL OF ENGINEERING
Department of Electrical Power Engineering and Mechatronics

DEVELOPMENT OF (HYBRID CORE)/CORELESS PCB MOTOR WITH RAPID MANNUFACTURING CAPABILITIES FOR DISPOSABLE DRONES

ÜHEKORDSELT KASUTATAVATE DROONIDE JAOKS MÕELDUD (HYBRID-CORE)/CORELESS PCB MOOTORI ARENDAMINE KIIRE TOOTMISVÕIMALUSEGA

MASTER THESIS

Student: Nawaf Ahmad

Student code: 21227MAHM

Supervisor: Muhammad Usman Naseer,
Early-Stage Researcher

Co-Supervisor Shahid Hussain,
Early Stage-Researcher

Tallinn, 2024

AUTHOR'S DECLARATION

Hereby I declare, that I have written this thesis independently.
No academic degree has been applied for based on this material. All works, majorviewpoints and data of the other authors used in this thesis have been referenced.

".....” ..... 202….

Author: .....
/signature /

Thesis is in accordance with terms and requirements

".....” ..... 20….

Supervisor: …....
/signature/

Accepted for defence

".....”.....20… .

Chairman of theses defence commission: .....
/name and signature/

Non-exclusive licence for reproduction and publication of a graduation thesis[2]

I, Nawaf Ahmad hereby

1. grant Tallinn University of Technology free licence (non-exclusive licence) for my thesis

"Development of (Hybrid-Core)/Coreless PCB motor with rapid manufacturing capabilities for disposable drones"

supervised by Muhammad Usman Naseer and Co supervised by Shahid Hussain

1.1 to be reproduced for the purposes of preservation and electronic publicationof the graduation thesis, incl. to be entered in the digital collection of the library of Tallinn University of Technology (TalTech) until expiry of the term of copyright;

1.2 to be published via the web of Tallinn University of Technology, incl. to be entered in the digital collection of the library of Tallinn University of Technology until expiry of the term of copyright.

2. I am aware that the author also retains the rights specified in clause 1 of the non-exclusive licence.

3. I confirm that granting the non-exclusive licence does not infringe other persons' intellectual property rights, the rights arising from the Personal DataProtection Act or rights arising from other legislation.

_____(date)

[2] *The non-exclusive licence is not valid during the validity of access restriction indicated in the student's application for restriction on access to the graduation thesis that has been signed by the school's dean, except in case of the University's right to reproduce the thesis for preservationpurposes only. If a graduation thesis is based on the joint creative activity of two or more persons and the co-author(s) has/have not granted, by the set deadline, the student defending his/her graduation thesis consent to reproduce and publish the graduation thesis in compliance with clauses 1.1 and 1.2 of the non-exclusive licence, the non-exclusive license shall not be valid for the period.*

TalTech Department's title
THESIS TASK

Student: Nawaf Ahmad , 215227MAHM

Study programme, MAHM02/18 MSc Mehatronics

Main speciality: Mechatronics

Supervisor(s): Muhammad Usman Naseer, Early-Stage Researcher

Consultant: Shahid Hussain, Early-Stage Researcher

Thesis topic:

Development of (Hybrid-Core)/Coreless PCB motor with rapid manufacturing capabilities for disposable drones

Kiire tootmisvõimalusega (hübriidtuum)/tuumita pcb mootori arendamine ühekordselt kasutatavate droonide jaoks

Thesis main objectives:

1. The primary objective of this thesis is to design, simulate, and prototype a PCB motor for drone applications that prioritizes lightweight construction and rapid manufacturing.
2. Theoretical Part: Electrical Machine Design, FEM simulations, Coreless motors, Axial Flux motors PCB design
3. Practical Part: Fabrication of PCB, 3D printing, assembling the motor, collecting the measurement data

Thesis tasks and time schedule:

No	Task description	Deadline
1.	Literature Review	20-Aug-2024
2.	Analytical Design and FEA simulations	1-Nov-2024
3.	Prototyping and Testing	20-Nov-2024

Language: English **Deadline for submission of thesis:** 19-Dec-2024

Student: ……. ..... "....."..... ....202….a

/signature/

Supervisor: ……. ..... "....."..... ....202….a

/signature/

Consultant: …….. ..... "....."..... ....202….a

/signature/

Head of study programme:

…….. ..... "....". 202….a

/signature

TABLE OF CONTENTS

PREFACE

I would like to thank Allah our creator for this gift of life and the chance every minute to live to the best and somehow be helpful for mankind.

I would like to appreciate and a big thanks to my supervisors Muhammad Usman Naseer and Shahid Hussain for mentoring and supporting me for working in a new field of knowledge through this thesis tasks. I would like to thank my family as well, for always supporting me and believing in me and continuous prayers from their side.

LIST OF ABBREVIATIONS

AFPM - Axial Flux Permanent Magnet

BLDC - Brushless Direct Current

CNT – Carbon Nanotube

CSAFPM- Coreless Stator Axial Flux Permanent Magnet

EMF- Electromotive Force

FEA - Finite Element Analysis

FEM - Finite Element Method

FOC - Field Oriented Control

HTS - High Temperature Superconducting

MRC- Magnetic Resonant Coupling

PCB - Printed Circuit Board

UAV - Unmanned Aerial Vehicles

YASA – Yokeless and Segmented Armature

1. INTRODUCTION

Global electricity demand is rising due to population growth and the increasing reliance on modern, power-dependent technologies. Innovations in transportation, renewable energy, and industrial automation rely on efficient electrical machines. Advancements in drones and aerial devices have further transformed industries such as logistics, agriculture, surveillance, and disaster response. A critical component in drone is the motor, which directly influences the drone's performance, efficiency, and versatility.

Conventional motors, though effective, are often limited by their weight, complexity, and manufacturing costs. In response, coreless axial flux motors have emerged as an ideal solution for drone applications due to their lightweight construction, high torque density, and should be easily manufacturable. Axial flux layouts provide better power-to-weight ratios in a compact design aspect, while coreless designs eliminate bulky ferromagnetic cores, lowering eddy current losses and increasing efficiency. These features make axial flux coreless motors particularly well-suited for small drones requiring high-speed operation and dynamic performance.

The integration of Printed Circuit Board (PCB) technology in motor design offers a promising solution. PCB motors, characterized by their compactness, reduced weight, and potential for cost-effective mass production, have gained increasing attention in recent years. Hybrid-core designs combine the advantages of traditional core-based and coreless motors, further optimizing efficiency and torque generation.

This thesis explores the development of a hybrid-core/coreless PCB motor tailored for disposable drone applications. The focus lies on scenarios which includes rapid manufacturing techniques to create a motor that is lightweight, efficient, and scalable for production. Through electromagnetic simulations and experimental performance testing, the study evaluates four distinct stator coil designs, comparing their performance against a conventional motor readily available in the market.

In the first part of this thesis application scenarios based coreless motors are discussed. Then analytical design of the machine design. The fundamental formulas used in the model will be explained. The third chapter also includes mechanical design of the stator and rotor which are major components of a motor part for construction of the prototype.

2 LITERATURE REVIEW

2.1 Electrical machines

Electrical machines are devices that convert electrical energy into mechanical energy, enabling the movement of various machines and systems across a wide range of industries. They play a vital role in modern technology and have diverse applications due to their ability to provide controlled motion. The pursuit of compact, lightweight, and rapidly manufacturable propulsion systems has intensified in recent years, particularly in the domain of small unmanned aerial vehicles (UAVs).

The demand for disposable drones used in short-term surveillance, monitoring, and delivery services continues to grow, engineers and researchers are seeking innovative motor designs that offer high torque density, reduced mass, and simplified assembly. Conventional motor designs often depend on heavy ferromagnetic cores and complex mechanical structures, which makes them less suitable for new lightweight and cost-sensitive applications.

This literature review will examine the progression of motor technologies, with particular attention to those that remove the traditional ferromagnetic core. By focusing on how coreless designs meet the demands of lightweight, rapid manufacturing, and cost-effective production, especially in emerging application scenarios like small, disposable drones, the review aims to highlight the technical and economic advantages driving current research and development in the field.

2.2 Emerging motor applications

Advancements in manufacturing technologies such as advent of additive manufacturing, printed electronics, and novel materials offer new methods for potentially producing electric motors at an unprecedented pace. In the aerospace and UAV sectors, especially in the field of small drones, the imperative is to reduce complexity and mass while retaining or even increasing the torque and speed capabilities[1]. High rotational speeds are critical for maintaining stable flight dynamics, efficient lift-to-thrust ratios, and agile maneuverability in drones[2]. Beyond UAVs, similar trends are emerging in other fields given below:

Robotics and Automation: Industrial robots and small-scale autonomous systems require motors that can be swiftly integrated into complex assemblies. Here, ease of manufacturing translates to faster prototyping and quicker pathway from design to deployment.

Consumer Electronics: Devices like small cooling fans, camera gimbals, and portable vacuum cleaners benefit from lightweight and compact electric motors. Rapid manufacturing makes it possible to frequently update designs and reduce lead times, thereby meeting fast-changing market demands.

Medical and Laboratory Instruments: In tools such as microfluidic pumps and surgical robots, motors must be both highly reliable and produced rapidly to meet urgent clinical or research needs. This calls for precise yet simplified manufacturing methods that reduce waste and ensure consistency across batches.

In each of these applications, a streamlined approach to motor fabrication can lead to improved performance, lower production costs, and the ability to quickly adapt designs as requirements evolve. As such, a shift toward materials and processes that eliminate unnecessary complexity becomes highly attractive.

2.3 Coreless motors

Coreless motors offer a unique combination of characteristics that align well with the needs of drone propulsion systems, especially in scenarios where rapid manufacturing, low cost, and light weight are key considerations. Unlike traditional motors that rely on heavy, solid ferromagnetic cores, coreless designs replace these dense components with lightweight, hollow structures[3]. This approach significantly reduces the mass of the motor, improving the power-to-weight ratio an essential factor in small drones that depend on efficient lift-to-weight performance[4].From a manufacturing standpoint, coreless motors simplify production processes. The absence of a metallic core also reduces eddy current losses, which can translate into higher overall efficiency and extended flight times, crucial given the limited onboard energy storage.

Coreless motors are known for their low rotational inertia and rapid acceleration characteristics[5]. For drones that must respond quickly to control inputs and maintain stable flight under turbulent conditions, the swift torque response enabled by coreless designs is highly desirable. In settings that require rapid deployment and potentially disposable equipment such as short-range surveillance drones or field monitoring devices coreless motors can streamline the supply chain and speed up production. By removing the core, material costs and manufacturing steps are reduced, making it easier to adopt integrated or semi-automated production methods. Cogging torque is also eliminated while maintaining a smoother operation. As a result, coreless motors are well-suited for applications that demand both high performance and quick, cost-effective manufacturing[6].

Coreless motors can be broadly classified into a few key types, each tailored to specific operating principles and performance requirements thus having advantages due to the reduction of ferromagnetic components to lower weight and improve efficiency[7]. Coreless brushed DC motors remove the iron core for lighter, more responsive operation. Coreless brushless DC motors extend these benefits by using electronic commutation instead of brushes, enhancing durability and control precision.

Linear variants apply the same principles to straight-line motion, improving accuracy in fields like semiconductor assembly. Slotless designs, though not fully coreless, still reduce cogging torque by eliminating traditional stator slots. PCB motors combine coreless motor designs with printed circuit board technology, creating lightweight and efficient propulsion systems ideal for disposable drones.

By fabricating the motor windings directly on the PCB and eliminating the traditional ferromagnetic core, these motors reduce weight and simplify the manufacturing process. This integration enables rapid and cost-effective production at scale, which is crucial for applications requiring quick deployment and large quantities[8].

2.4 Existing researches

To begin exploring the applications mentioned, the literature review of existing research and technologies should first focus on coreless motors. This involves examining how various coreless motors have been designed and analyzing the studies conducted on different aspects of these motors. This approach is crucial for understanding the lightweight characteristics of these machines.

This research paper[9] presents the design, simulation, and performance analysis of a coreless axial flux permanent magnet brushless motor (PMBM) tailored for high-efficiency applications. The motor utilizes a disk-type configuration without ferromagnetic cores, employing a Halbach array of permanent magnets to achieve a high airgap flux density exceeding 0.6 Tesla. Finite Element Method (FEM) simulations validated the electromagnetic performance, confirming the targeted flux density and efficient torque generation. A 10 kW motor prototype demonstrated approximately 1% higher efficiency and 82% greater power density compared to conventional cylindrical motors with laminated cores.

Experimental tests confirmed the simulation results, highlighting the motor's superior performance and reduced mass. The coreless design eliminates cogging torque and minimizes eddy current losses, enhancing overall efficiency. However, the high cost of manufacturing and challenges in scaling the design for larger motors remain areas for improvement. Future research could focus on optimizing material costs, enhancing manufacturing techniques for mass production, and exploring advanced magnet configurations to further increase performance metrics. This research has given the opportunity to firstly understanding the design concept of the coreless PM brushless motor what steps and techniques are to be used for the machine design and overall. This machine significantly high performance as comparison to the conventional cored machine but production cost increased to 109.3% as discussed in the paper which is a pessimistic feature for a key application scenario.

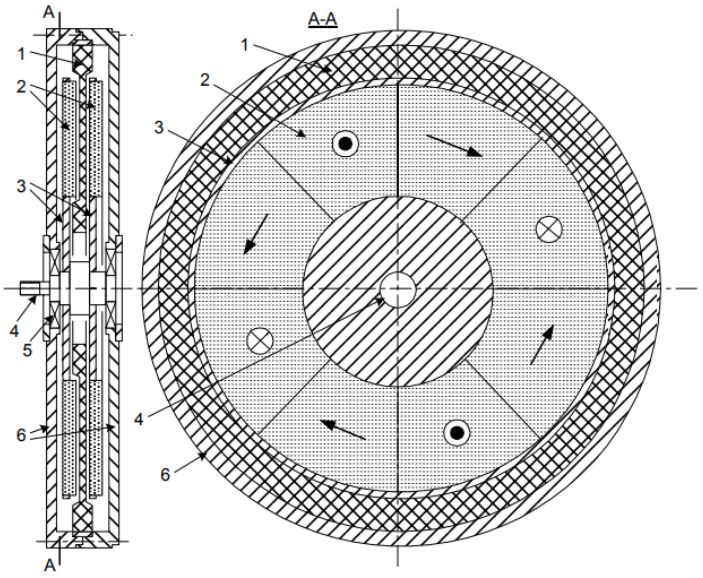

Figure 2.1 Disk Type coreless PMBM 1-coreless stator, 2-PM's, 3-twin Rotor, 4-Shaft, 5-Bearing, 6-Frame. This figure is given and explained in the avoe discussed research[9]

In this paper[10] The WAVED motor, a coreless axial flux PM machine with two phases and wave windings, is designed for traction applications, offering high efficiency and reduced mass by eliminating core losses. Utilizing 3D FEA optimization, it achieves superior high-speed performance with innovative flux control via stator rotation for constant power operation. Its fault tolerance is enhanced through magnetic decoupling of phases, and it achieves competitive efficiency compared to conventional motors like the YASA P400. Future improvements could focus on enhancing efficiency, extending speed range, optimizing costs, and exploring broader applications. As this approach is non-conventional and requiring complex driving circuits automatically negates the purpose of ease of manufacturability.

This research paper[11] introduces a novel core-less multi-layered axial flux brushless motor designed to eliminate cogging torque while enhancing torque output. By alternately stacking multiple permanent magnet (PM) layers and coil layers in the axial direction, the motor increases the flux density reaching the coils, thereby improving torque. Three-dimensional Finite Element Analysis (FEA) was employed to investigate the relationship between torque and the PM-to-coil ratio, the number of layers, and the outer diameters of the PM and coil layers. The simulations revealed that an optimal PM ratio of around 50% maximizes torque, and increasing the number of layers consistently boosts torque up to a saturation point. An experimental prototype with a coil layer outer diameter of 110 mm

confirmed that the multi-layered structure effectively increases magnetic flux density and torque. Future improvements should focus on prototyping the motor, optimizing layer configurations for even greater performance, and developing cost-effective manufacturing methods to enable large-scale production. Since the prototype is not developed so there is no power rating speed and torque rating of the machine but there lies a concept that layering either stator coils or rotors in a certain ratio can maximize torque of the machine. This is method should be validated only after the prototype as been developed so that practical limitations and thermal management issues can be addressed. Investigating cost effective design while making it viable and scalable for different power and torque requirements.

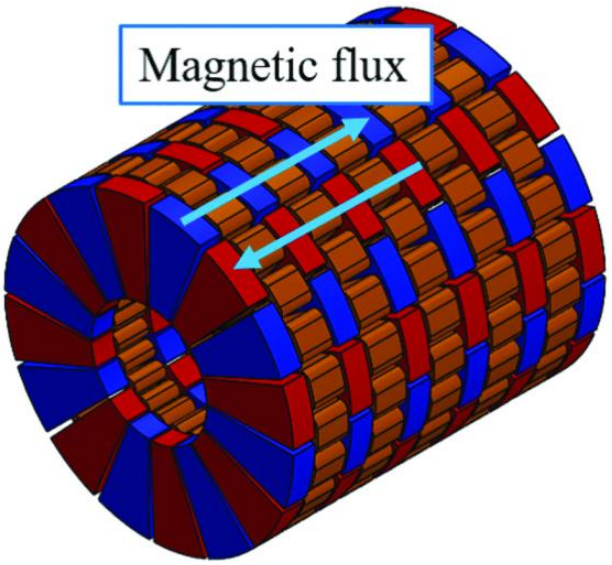

Figure 2.2 Multi-layered axial motor cad model taken form the discussed research [11]

This research[12] compares a multilayer printed circuit board (PCB)-based coreless axial flux permanent magnet (AFPM) motor with a conventional laminated-core-stator AFPM motor for high-speed, low-power applications. The PCB motor offers higher efficiency (94% vs. 91%), reduced cogging torque, and compactness by eliminating stator core losses but faces challenges like reduced flux linkage and higher thermal rise. Simulations and prototype testing validated these findings, highlighting its potential for compact, efficient motor applications. Improvements could include enhanced cooling for thermal management, advanced materials for better thermal and mechanical balance, designs to boost flux linkage, cost-benefit optimization for industrial use, and evaluations for broader applications such as robotics and aerospace. The power rating, output torque, power density and type of motors are given in the table 2.1.

This paper [13] investigates three different radial flux ironless BLDC (Brushless DC) motor topologies: one without inner back-iron, one with inner back-iron, and one with a dual-rotor configuration. By using finite element analysis (FEA), the authors compare their magnetic field distribution, back-EMF waveform quality, axial end effects, and torque characteristics. The results show that the dual-rotor topology provides a higher magnetic flux density and potentially better torque performance. Meanwhile, the winding configuration and slot-pole combinations significantly affect back-EMF and torque ripple. Axial end effects must also be considered for accurate performance predictions. Although one motor type shows better overall performance, further work could explore different magnetization patterns (e.g., Halbach array), enhanced cooling strategies, or advanced winding configurations shown in Fig 2.1. Future improvements might include optimizing magnet shapes, refining winding layouts for more ideal EMF waveforms, and implementing more sophisticated control schemes to reduce torque ripple and improve efficiency.

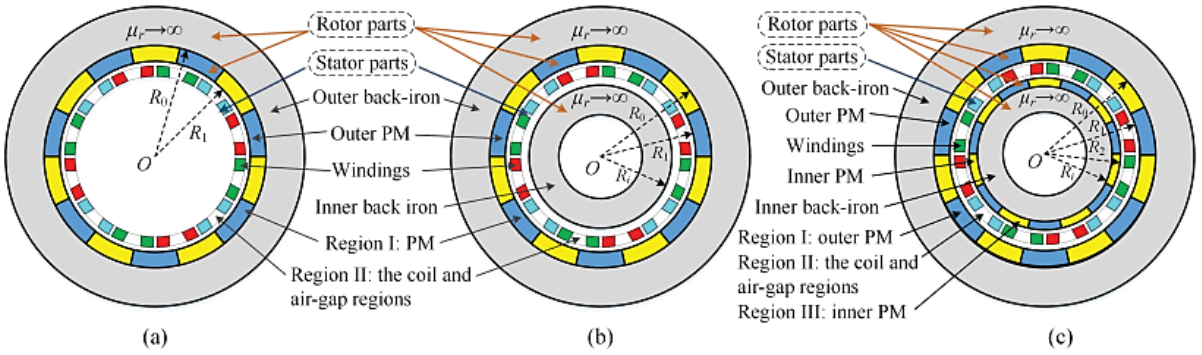

Figure 2.3 This is comparison view of the models of three different ironless BLDC types[13]

This paper [14] presents the design, analysis, and experimental validation of a high-speed, low-power, coreless axial-flux permanent-magnet (AFPM) motor featuring a printed circuit board (PCB) stator winding. The motor is designed to operate at 30,000 rpm and deliver approximately 62.8 W output power with a rated torque of 0.02 Nm. A Halbach-array permanent-magnet rotor is employed to enhance air-gap flux density and reduce magnet volume. The coreless PCB stator minimizes iron losses and enables a compact, efficient design. Finite element analyses and experimental tests confirm that the proposed motor achieves sinusoidal back-EMF, low torque ripple, and a high efficiency (~94%). Sensorless field-oriented control (FOC) demonstrates stable operation at high speeds. Future work could focus on further reducing eddy current losses in the stator's metallic parts, refining the control algorithm at very high speeds, and using lighter, non-conductive support

materials to minimize additional losses. Additionally, integrating advanced bearing systems or magnetic bearings might allow safe and reliable operation beyond 25,000 rpm and fully leverage the design's potential. The power rating, output torque, power density and type of motors are given in the table 2.1.

The authors present [15] a novel approach to electric motor design that completely the use of ferromagnetic materials and permanent magnets. Instead, their motor employs magnetic resonant coupling (MRC) between carefully tuned coils on the stator and rotor. Through analytical modeling, finite element simulations, and a physical prototype, the research demonstrates that this magnet less, coreless configuration can successfully transfer electromagnetic energy at a resonant frequency to produce torque. Experimental tests validate the basic feasibility, though the initial performance metrics remain modest compared to conventional motors. The paper identifies opportunities for further optimization, including higher-quality coil materials, improved coil geometry, and advanced control schemes. These improvements could eventually enhance the motor's torque and efficiency, offering a lighter, potentially more sustainable, and cost-effective alternative to traditional designs. The power rating, output torque, power density and type of motors are given in the table 2.1.

The paper [16] compares two types of axial flux permanent magnet (AFPM) motors one with a conventional stator core and one that is coreless for use in solar-powered vehicles. The study shows that both the conventional and coreless configurations can meet the torque requirements, but each has unique advantages: the conventional AFPM can be optimized for a single driving wheel with lower overall mass and losses shown in Fig 2.2 and Fig 2.3, while the coreless AFPM is well suited for a two-wheel drive approach, providing better mass distribution. Although the coreless design may have slightly lower efficiency at the rated speed, it benefits from the absence of cogging torque and lamination losses, and thus may outperform the conventional design at higher speeds. Future work could investigate advanced cooling methods, materials with higher fill factors or better thermal properties, and refined winding techniques (e.g., special Litz wire configurations) to further reduce losses, especially at high speeds. The power rating, output torque, power density and type of motors are given in the table 2.1.

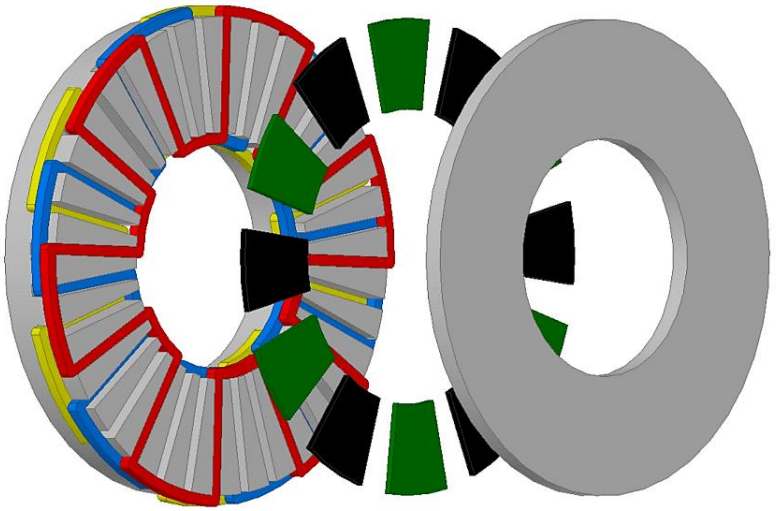

Figure 2.4 Exploded view of the 3-D model of the motor with 36 stator slots and 12 rotor poles[16]

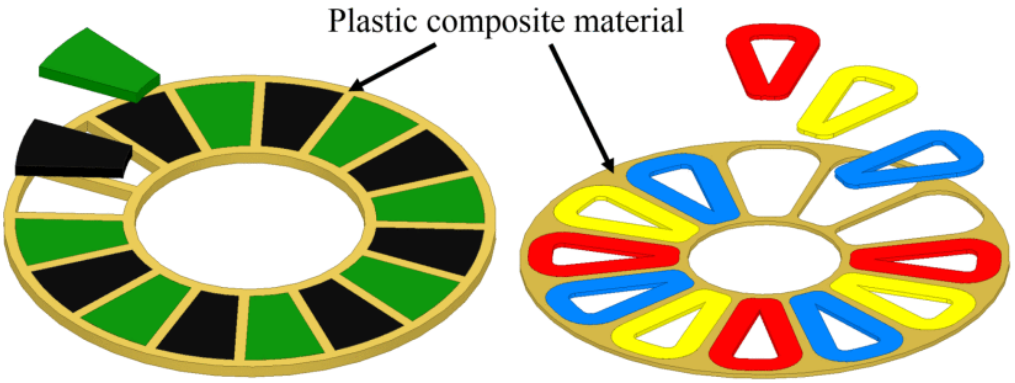

Figure 2.5 Schematic of a coreless stator and rotor employing a plastic composite structure for mounting and supporting magnets and coils[16]

This study [17] presents a high-temperature superconducting (HTS) coreless induction motor that uses saddle-shaped HTS coils and a standard squirrel-cage rotor to achieve lightweight, high-speed performance. Electromagnetic analyses show that optimizing coil arrangements reduces perpendicular magnetic fields on the HTS tapes, maintaining higher critical current and improving performance. The resulting design lowers torque ripple and improves air-gap flux distribution, offering a promising path toward advanced high-speed, high-power HTS motors shown in Fig 2.4. Further research could focus on refining coil winding techniques to minimize tape bending stress, testing the motor under various load and speed conditions, and exploring advanced cryogenic cooling strategies. Additionally,

practical assessments of mechanical integrity at very high speeds and the integration of improved rotor designs or materials would aid in pushing power density and stability even further. The power rating, output torque, power density and type of motors are given in the table 2.1.

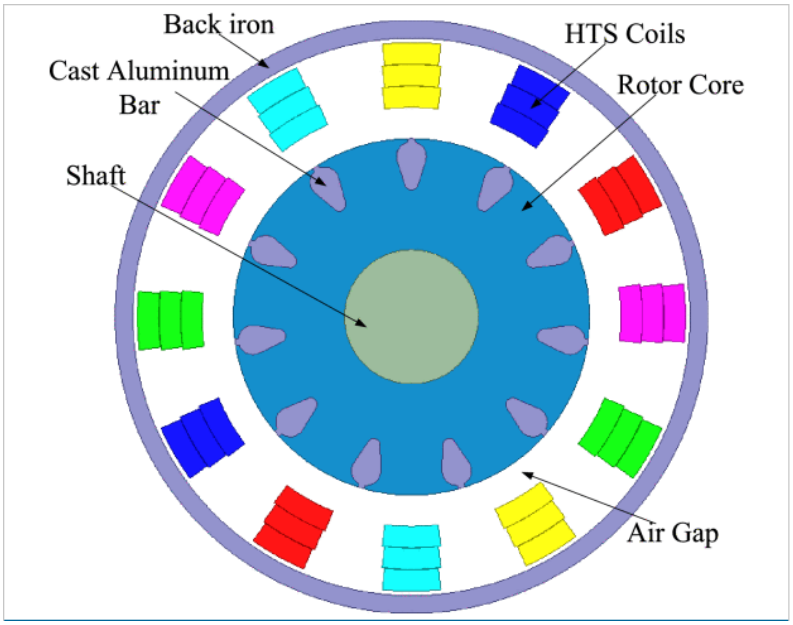

Figure 2.6 Basic structure model of HTS CIM[17]

This paper [18] evaluates the feasibility of using carbon nanotube (CNT) conductors instead of copper in a coreless axial flux permanent magnet (AFPM) motor with multidisc construction. By leveraging CNT's low mass density, negligible skin effect, and reduced temperature coefficient of resistance, the study shows that at higher speeds and frequencies, CNT windings can achieve higher power density with comparable volume than conventional copper windings. The authors apply sizing equations, finite element analysis (FEA), and parametric comparisons to confirm that CNT-based designs can notably improve power-to-mass ratios, especially for high-speed applications shown in Fig 2.5. Future work could focus on improving CNT conductivity, refining manufacturing processes for CNT wires, validating high-frequency operation with experimental prototypes, and integrating advanced cooling methods to fully realize the potential of CNT-based windings. The power rating, output torque, power density and type of motors are given in the table 2.1.

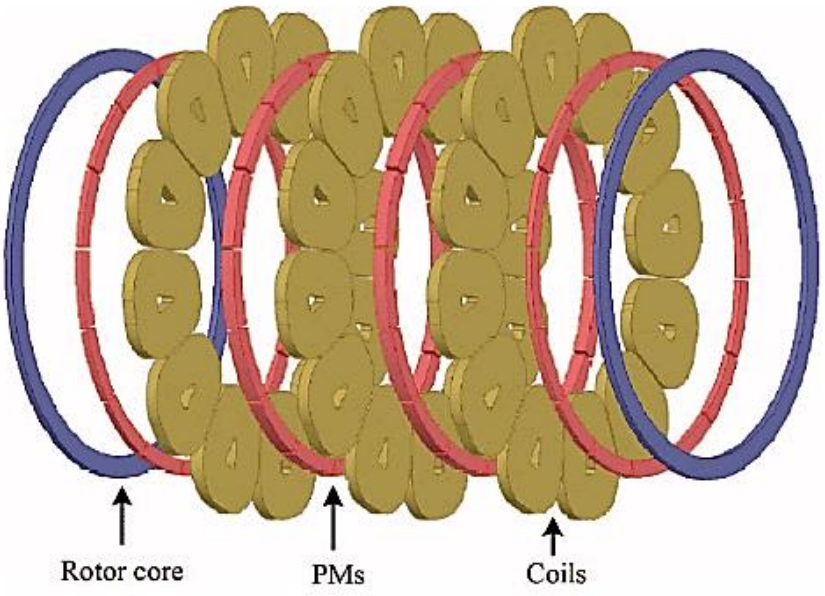

Figure 2.7 Components of the proposed coreless AFPM machine. Supporting discs for the stator coils and rotor PMs are not shown for clarity[18]

This research [19] paper presents a comprehensive comparison of various stator winding technologies for coreless axial flux permanent magnet (AFPM) machines, focusing on their impact on efficiency, torque density, and manufacturability. By analyzing traditional round or Litz wire windings alongside more advanced solutions such as PCB, anodized aluminum strips, ceramic-PCB substrates, and additive manufacturing, the authors identify suitable approaches for both low-speed, high-torque applications and high-speed operations where AC losses and thermal management are critical. The results highlight the trade-offs between copper fill factors, eddy current losses, and ease of production, offering guidelines for selecting the optimal technology based on specific design requirements shown in Fig 2.6. Future developments could explore improved winding materials, higher temperature capabilities, refined manufacturing techniques for complex geometries, and scaled production methods that integrate advanced substrates or 3D printing for more efficient and robust AFPM machines. This research discussed various stator windings and different materials which can be used to improve the stator windings but the prototyping was not considered in this research. The power rating, output torque, power density and type of motors are given in the table 2.1.

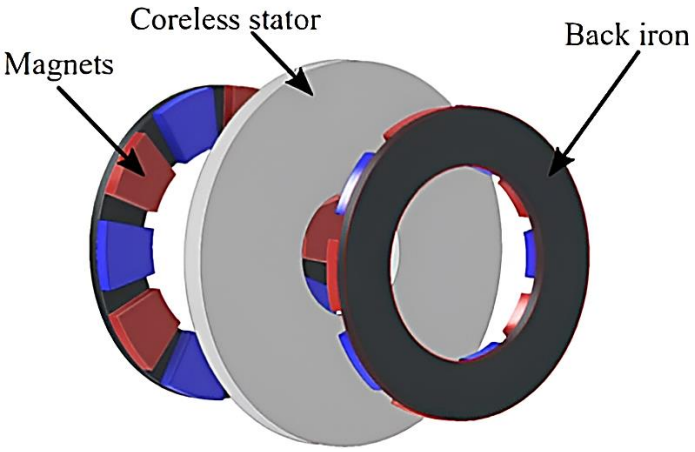

Figure 2.8 3D exploded view of the coreless axial-flux permanent-magnet machine[19].

This research [20] presents a design and optimization process for a coreless stator axial-flux permanent magnet (CSAFPM) in-wheel motor intended for unmanned ground vehicles. By integrating a planetary reducer and using a Halbach-array PM rotor configuration, the motor achieves high torque density and efficiency within tight spatial constraints. The authors employ multiphysics approaches, including electromagnetic, mechanical, and thermal analyses, along with finite element modeling and response surface methods, to optimize key parameters such as rotor geometry and stator support structures. A 35 kW prototype was built and tested, demonstrating improved torque performance, reliability, and reduced weight shown in Fig 2.7. Future work could explore more advanced materials, refined cooling solutions, or further optimization techniques to enhance power density, reduce losses, and improve overall system integration. The power rating, output torque, power density and type of motors are given in the table 2.1.

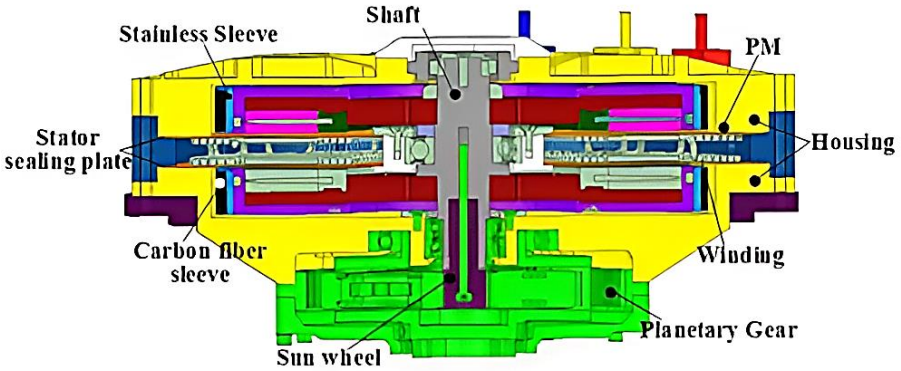

Figure 2.9 Structure of ID in-wheel motor[20]

This research [21] paper introduces and validates a high-strength, oil-immersed cooling stator design with nonoverlapping concentrated windings specifically tailored for high-power ironless stator axial-flux permanent magnet (AFPM) machines shown in Fig 2.8 and Fig 2.9. By leveraging a specialized winding configuration, epoxy-based stator supports, and a forced oil cooling system integrated into the stator's structure, the design achieves improved thermal performance, enhanced mechanical stability, and strong short-term overload capabilities. Numerical analysis and finite element simulations guide the selection of key parameters, while a 50-kW, 9000-rpm prototype demonstrates the system's high efficiency, manageable temperature rise, and overall feasibility shown in Fig 2.10 and Fig 2.11. Future improvements could focus on refining coil arrangements for even higher winding factors, exploring advanced materials with better thermal conductivity and mechanical properties, and further optimizing the cooling channels to push efficiency and power density limits. The power rating, output torque, power density and type of motors are given in the table 2.1.

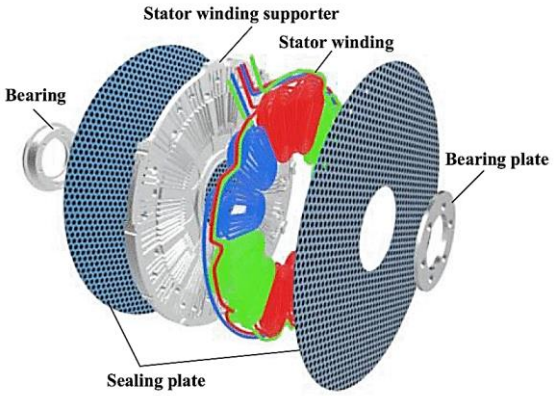

Figure 2.10 Oil-Immersed cooling ironless stator[21]

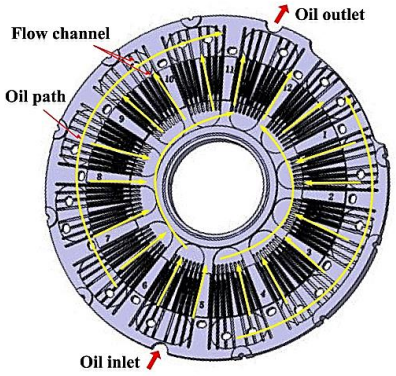

Figure 2.11 Whole structure and cooling system design(right)[21]

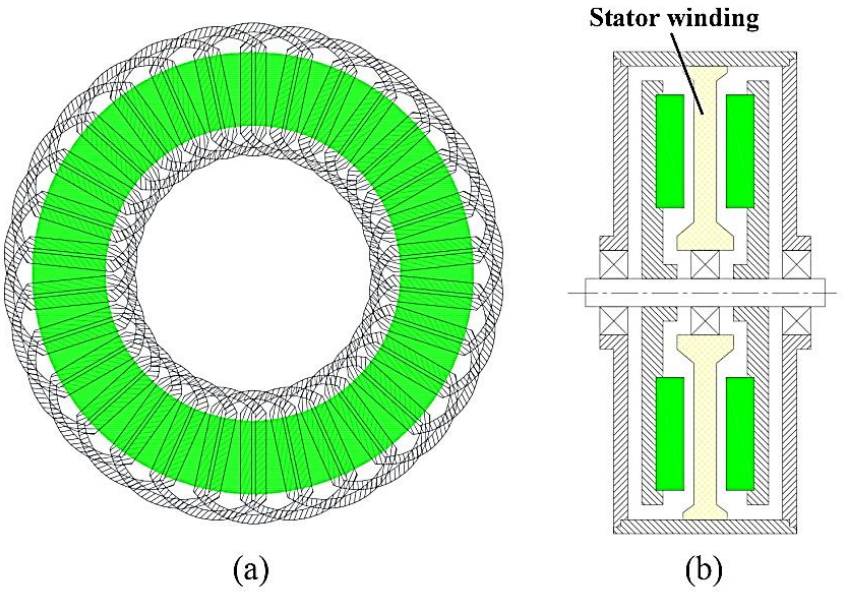

Figure 2.12 Basic structure of AFPM machine with overlapping distributed winding. (a) Stator winding configuration. (b) Assembly diagram[21]

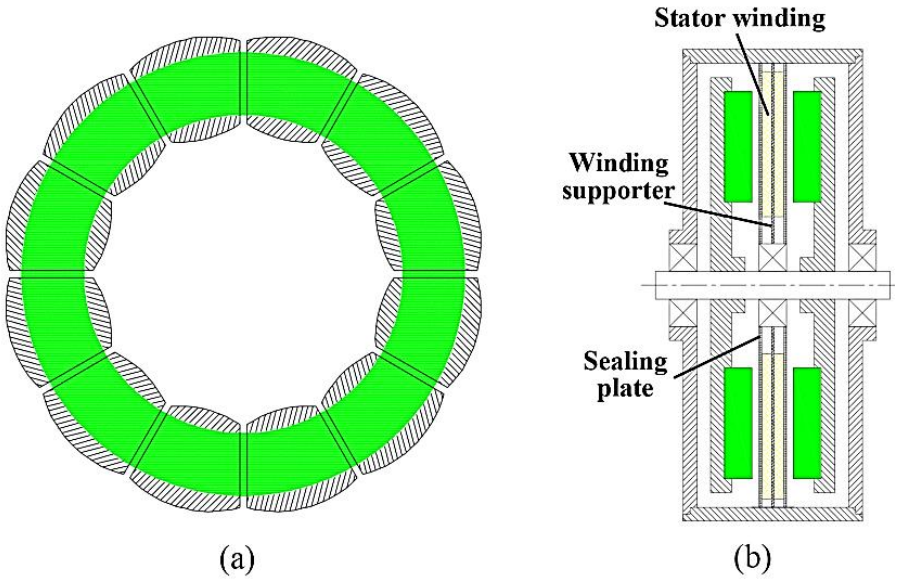

Figure 2.13 Basic structure of AFPM machine with nonoverlapping concentrated winding. (a) Stator winding configuration. (b) Assembly diagram[21]

Table 2.1 provides an overview of various coreless motors designed in previous studies, showcasing the different technologies used. A primary focus in these designs was to ensure that coreless motors were easy to manufacture and cost-effective. Most of the motors employed axial flux topologies and aimed to improve power and torque. However, these enhancements often resulted in more complex designs and increased weight, which undermined the benefits of a coreless structure. The information in the table was gathered from the literature reviewed above.

Table 2.1: Displays the data of different coreless motors

Type of motor	**Power Rating**	**Speed**	**Torque**	**Power Density**	**Torque Density**
Coreless AFPM PCB stator	62.8 W	30,000 rpm	0.02 Nm	n/a	n/a
Coreless AFPM Brushless Motor	10 kW	n/a	131 Nm	444.25 W/kg	n/a
Coreless Multi disk AFPM	1.17 kW	400 rpm	28 Nm	n/a	n/a
HTS Coreless induction Motor	18 kW	n/a	30 Nm	n/a	n/a
Coreless AFPM Multidisc	2.2 kW	n/a	20 Nm	n/a	n/a
Coreless PM Synchronous Motor	790 W	n/a	3.51N.m	n/a	n/a
Coreless AFPM	n/a	n/a	5 Nm-1.2 Nm	n/a	n/a
Corless magnet less	50 W	n/a	0.15 Nm	n/a	0.05 Nm/kg
Ironless Stator AFPM	50 kW	n/a	n/a	11.3 kW/kg	10.6 Nm/kg
Coreless AFPM Motor with PCB Stator	62.8 W	n/a	0.02 Nm	n/a	n/a
Coreless Stator AFPM	35 kW	n/a	1100 Nm	29.8 Nm/kg	n/a
Coreless magnet less	50 W	0.15 Nm	n/a	0.05 Nm/kg	n/a

2.5 Axial flux vs radial flux

In the context of small unmanned aerial vehicles (UAVs), axial flux motors offer several key advantages over radial flux motors that make them particularly well-suited for drone applications. Axial flux designs typically provide higher torque density and better power-to-weight ratios, which are essential for drones that need to be lightweight yet powerful. The flat, disk-like shape of axial flux motors allows for a more compact and streamlined integration into drone frames, accommodating the short propeller sizes and limited space available in small drones[22].

Axial flux motors can be easily manufactured using coreless and PCB-based techniques, which simplifies the production process and reduces costs. This is especially important for disposable drones, where rapid and cost-effective manufacturing is crucial. The absence of a heavy iron core in axial flux motors not only reduces the overall weight but also lowers rotor inertia, resulting in faster response times and more agile maneuvers key attributes for high-speed and responsive drone operations[16], [23].

Furthermore, axial flux motors exhibit superior thermal management capabilities compared to radial flux motors. Their flat, disk-like geometry provides a larger exposed surface area relative to their volume, enabling more efficient heat dissipation. This enhanced thermal performance helps maintain optimal motor temperatures during prolonged or intense operation, ensuring consistent performance and reliability.

In contrast, the compact, cylindrical design of radial flux motors limits their ability to effectively dissipate heat, which can result in higher operating temperatures and reduced efficiency in high-demand applications[23]. Overall, the combination of higher torque density, lightweight construction, compact form factor, and compatibility with advanced manufacturing methods makes axial flux motors a superior choice for UAV applications. These benefits align perfectly with the requirements of modern drones, making axial flux motors an emerging preference over traditional radial flux designs.

3 DESIGN METHODOLOGY

3.1 Conceptual approach

The fundamental principle governing torque production in electric machines is the Lorentz force. When a conductor carrying an electric current is placed within a magnetic field, it experiences a mechanical force. For a single conductor segment of length $\boldsymbol{l}$ carrying current I and subjected to a magnetic flux density $\boldsymbol{B}$, the Lorentz force $\boldsymbol{F}$ is given by:

$$F = I(L \times B)$$

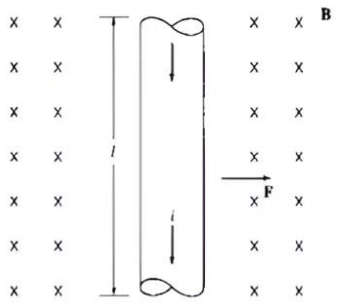

Fig. 3.1: A current carrying conductor within a magnetic field[24]

According to the right-hand rule, when the magnetic field is directed outward and the current flows downward through the conductor, the resulting Lorentz force acts towards the right as shown in Fig. 3.1. If we consider a conductor lying along a certain direction, the direction and magnitude of the force depend on the orientation of the magnetic field with respect to the conductor. In a rotating machine, the torque T can be considered as the summation (or integral) of all these incremental forces acting tangentially to the rotor's circumference:

$$\mathrm{T} = \sum(\mathrm{r} \times \mathrm{F}) \text{or, in continuous form,} \mathrm{T} = \int \mathrm{rdf} \tag{3.1}$$

where r is the radius at which the force acts. Given the rotor structure and the uniform arrangement of phases, a well-designed stator winding ensures that the resultant torque is smooth and predictable.

3.1.1 Influence of conductors and current density

Torque production in an electric machine can be enhanced by either:

- Increasing the magnetic flux density B in the airgap.
- Increasing the current I in the stator conductors.
- Increasing the effective length of conductors interacting with the flux (i.e., optimizing coil layout and fill factor).

In a coreless configuration, the airgap flux density is inherently limited by the absence of an iron core. This places a stronger emphasis on increasing the current-carrying capacity of the stator windings. The torque T, at its simplest form when focusing on a single coil region, can be approximated as:

$$T \propto B \cdot I \cdot leff \tag{3.2}$$

Here, $leff$ represents the effective conductor length in the active region. Since B cannot be substantially increased without a core, and $leff$ is constrained by the machine geometry, the main variable we can influence is I. The current I depends on the conductor's cross-sectional area and material properties. This is where the concept of copper fill factor and linear current density becomes critical.

A typical approach to increase back-EMF or voltage rating in a motor is to add more turns per coil. However, each additional turn requires spacing and clearance between tracks, reducing the effective copper fill factor. In other words, as the number of turns increases, a greater fraction of the available perimeter space is taken up by clearances between the traces, not contributing to current conduction.

By considering only one turn per coil, the available copper area for that turn is maximized. A single, wide copper track can occupy the entire allotted slot area without the need for multiple parallel traces and clearances between the traces. This approach maximizes the copper fill factor and substantially increasing the cross-sectional area of conductive copper within the same geometric constraints

As the linear current density in m-phase rotating electrical machines can be mathematically expressed as

$$A_s = \frac{2mN_t I}{\pi D} \tag{3.3}$$

where m is the number of phases, N_t is the number of turns per phase, I is the phase current, and D is the effective diameter at the mid-airgap. From the above equation (3.3) the increase in conductor cross-sectional area enables higher phase current I without exceeding thermal or material limits. Although the number of turns N_t is minimized, the enhanced current-carrying capacity of the single wide copper track compensates for this reduction, allowing A_s to be even improved due to the higher current and copper fill factor. By further increasing the linear current density, multiple layers can be incorporated into the PCB stator of the same thickness. For example, employing a six-layer PCB stack-up, each layer maintains the same current-carrying capacity as a single-layer configuration. However, when these layers are combined, the total current rating increases proportionally to the number of layers, effectively increasing the overall ampere-conductor product.

This approach further improves the linear current density As, thereby enhancing the motor's torque production capability. Having established the relationship between linear current density, copper fill factor, and the advantages of multiple layering, careful consideration must now be given to the selection of stator and rotor pole combinations. Based on the winding factor, which directly affects the induced EMF waveform and torque characteristics, choosing an optimal pole configuration ensures that the improvements in current capacity and conductor utilization are effectively translated into enhanced overall motor performance. From Fig. 3.2, certain combinations such as a 9/10 stator/rotor pole combination, offer particularly high winding factors. However, design constraints on the rotor may limit the feasibility of this combination which can be discuss later. Under such design considerations, a 15/16 combination emerges as an optimal choice that closely approaches the winding factor performance of the 9/10 combination.

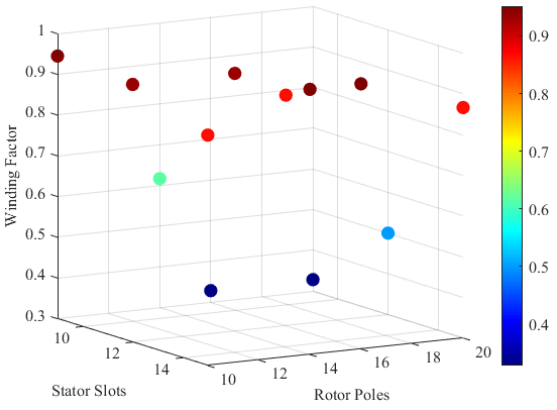

Fig. 3.2: Winding factor on different stator rotor pole combinations

3.2 Rotor design

The rotor design process begins with defining a target airgap flux density, which serves as the basis for magnet selection and arrangement. This dimensioning takes into account the magnet's recoil permeability (μr), remanence flux density (Br), leakage factor (Kl), and reluctance factor (Kr). The concentration factor (cφ) also plays a role, as it relates the flux density at the magnet's surface to that in the airgap. The magnet axial length l_{pm} can be determined from:

$$l_{pm} = \frac{u_r . B_{av} . g . K_r}{K_l . B_r - \frac{B_{av}}{c_\emptyset}} \tag{3.4}$$

Once the target flux density is set, the chosen magnet type and dimensions must be compatible with both the PCB rotor substrate and the overall mechanical structure. The rotor is typically fabricated as a PCB with precision-drilled holes that securely hold cylindrical disc magnets. Ensuring stable seating of these magnets is vital for maintaining a uniform airgap and consistent flux distribution.

In many BLDC PCB motor designs, wedge-shaped magnets are preferred due to their ability to provide a nearly uniform flux distribution. However, producing custom wedge magnets increases cost and complexity. To address this, two differently sized disc magnets can be employed to approximate the flux characteristics and area coverage of a single wedge magnet. Using standard disc magnets significantly reduces lead times and expenses associated with custom magnet fabrication.

The number of stator and rotor poles is selected based on achieving a favorable winding factor and accommodating the chosen magnets as discussed earlier. A higher winding factor typically yields more efficient electromagnetic coupling and improved back-EMF characteristics. While a 9/10 stator rotor pole combination offers a slightly higher winding factor than other configuration like 15/16, but it poses practical limitations in terms of magnet arrangement. With a 9/10 setup, the pole area cannot be fully covered by the combination of two-disc magnets, resulting in suboptimal flux utilization and reduced uniformity.

In contrast, the 15/16 stator rotor pole combination achieves an effective balance between winding factor and practical rotor design considerations. For this configuration, two-disc magnets of carefully selected sizes can fully cover the magnetically active pole area, approximating the performance of a wedge magnet. Fig 3.3. illustrates the placement of two-disc magnets with different diameters on a single rotor pole for the 15/16 combination. The combined magnetized area closely matches that of a wedge magnet designed for this configuration, maintaining a uniform flux distribution. By selecting this pole combination and employing two-disc magnets instead of a single wedge magnet, it is possible to approximate the intended flux distribution without incurring the higher costs, limited supplier availability, and increased lead times for custom shapes.

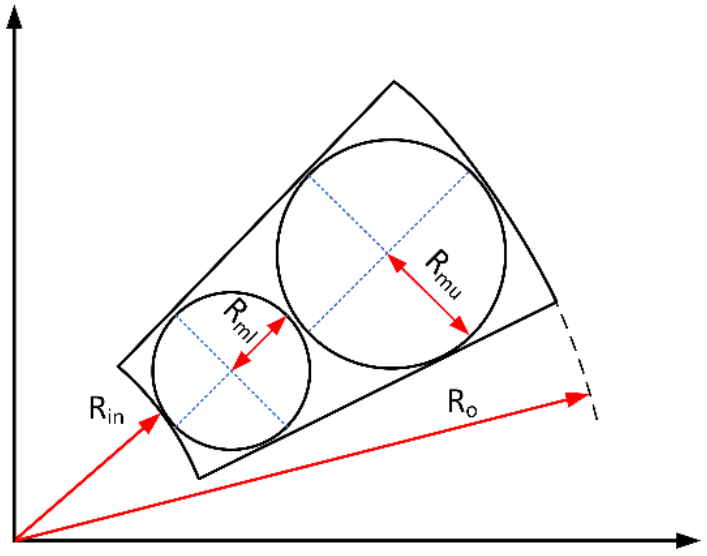

Fig. 3.3: Magnets representation for one rotor pole

3.3 Stator design

With the rotor's flux distribution established, the stator must be designed to maximize linear current density and effectively convert the available magnetic field into torque. This is accomplished through careful selection of winding topology, conductor dimensions, and layer configurations on the PCB stator. A wave winding scheme is employed, where each coil is connected in series with the adjacent coil in an alternating direction.

This arrangement ensures that the magnetic fields from each coil add constructively, improving the overall performance. A single-line diagram illustrating the wave winding layout is provided in Fig. 3.4. By utilizing this winding configuration, the stator can achieve a balanced distribution of phases around the circumference, leading to a more uniform back-EMF waveform and smoother operation.

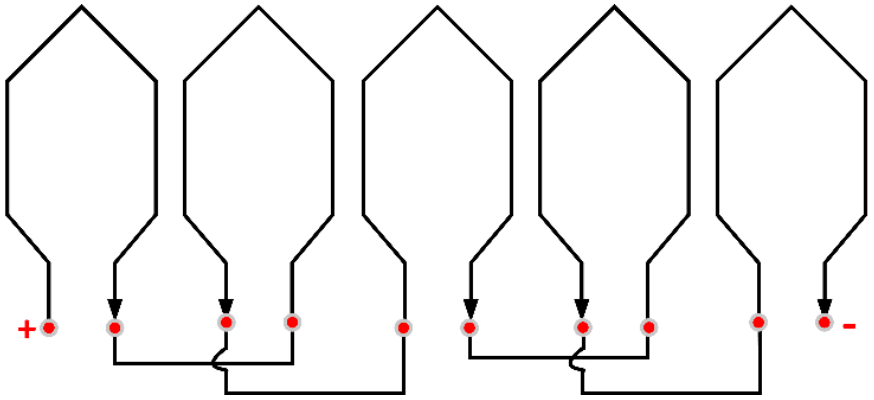

Fig. 3.4: Winding layout for one phase of PCB stator

Unlike conventional approaches that increase the number of turns to raise the back-EMF, here only one turn per coil is used. This simplifies the geometry, eliminating the need for multiple parallel copper tracks and their associated clearance gaps. As a result, a single, wide copper trace can occupy the entire coil slot area, maximizing the copper fill factor. This approach significantly increases the conductor's cross-sectional area and, consequently, the current-carrying capacity per coil. To further boost the current-handling capability without increasing the number of turns, multiple copper layers are incorporated into each stator board.

In this design, each PCB stator side consists of six copper layers connected in parallel through vertical interconnect access (vias). Although still representing one electrical turn per coil, these multiple layers collectively provide a larger effective cross-sectional area, thereby allowing higher currents to flow without excessive resistive losses. This design choice keeps the back-EMF relatively low, enabling the motor to operate at higher currents and lower voltages, which can be advantageous in applications such as drones, where battery voltage levels are often flexible. Each stator PCB layer has a copper trace width (tw) of 1.5 mm and a thickness (tc) of 0.07 mm. The clearance between adjacent traces is maintained at 0.3 mm to ensure proper insulation and manufacturability.

Additionally, there is a 0.11 mm gap between the layers, preserving the structural integrity of the PCB and providing adequate dielectric spacing. Table 1 summarizes these key design parameters, along with the chosen motor dimensions and magnet specifications.

When multiple copper layers are used per phase, each layer carries current from the start of the winding path. As the current progresses through the coils, it eventually transitions from the second layer to the first layer via interconnecting vias. At this transition point, the current from the two layers merges, effectively doubling the total current within a single conductor segment of the first layer.

To prevent an excessive rise in current density and associated heating, the conductor width in that section must be increased. By providing approximately twice the cross-sectional area where the currents combine, the current density remains consistent with other segments of the winding that carry current from only one layer.

As the current completes the coil in the first layer and moves on, a similar process of distribution, merging, and conductor resizing repeats for subsequent coils and layers. Fig. 3.5 shows how the copper track geometry is adapted to handle these varying current levels. By increasing the conductor width in areas where multiple layer currents merge, the design will ensure uniform current distribution, controlled thermal conditions, and reliable operation under the desired load scenarios.

Table 3.1: Motor and PCB design Parameters

Parameters	**Value**	**Unit**
Outer diameter	40	mm
Inner diameter	9	mm
Trace width	1.5	mm
Trace thickness	0.07	mm
Clearance between traces	0.3	mm
Upper magnet diameter	6	mm
Lower magnet diameter	4	mm
Single PCB layers	6	-
Gap between layers	0.11	mm
Rated Speed	30000	rpm
Airgap length	0.5	mm
Magnet length	3	mm
Copper thickness/layer	0.07	mm
Magnet type	N52	-

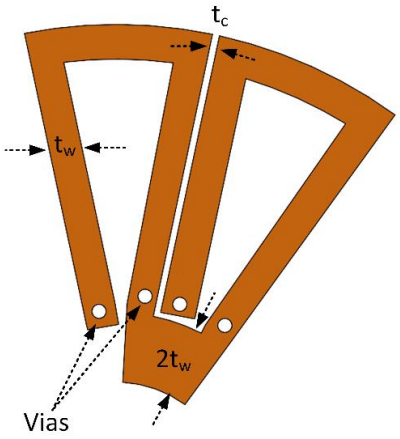

Fig. 3.5 Representation of one trace pair

3.4 Dual stator configuration

In a coreless axial flux BLDC design, the absence of ferromagnetic materials in the stator and rotor back-iron means the flux paths are not channeled as effectively as in conventional machines. To address this limitation and enhance torque production, a dual stator configuration is adopted. By placing one stator on each side of the rotor, the magnetic flux generated by the rotor magnets interacts with stator conductors on both faces of the rotor disc.

In a single stator arrangement, only one side of the rotor's magnetic field would be actively contributing to torque generation. However, with a stator on both sides, the rotor's magnets now face two sets of coils, effectively doubling the active area available for flux interaction. This ensures that the rotor's magnet flux is not wasted on the non-active side and is instead utilized to produce additional electromagnetic force. As a result, the torque density improves without needing to increase magnet size, magnet grade, or the current beyond what has already been optimized at the stator level.

The dual-stator approach inherently creates a more symmetric structure. With stators on both sides, axial forces from the magnets tend to balance out, reducing the net force on the bearings. This mechanical equilibrium contributes to smoother operation and potentially longer bearing life. The symmetrical design also simplifies assembly and alignment

procedures, as each stator can be positioned with respect to the rotor to ensure minimal runout and uniform airgap distribution on both sides.

As conventional axial flux machines often rely on back-iron (ferromagnetic return paths) to concentrate and guide the magnetic flux through the coils. In this design, the absence of a ferromagnetic stator core and rotor back-iron means the flux naturally disperses more widely. The dual-stator arrangement partially compensates for this dispersal by effectively catching flux lines on both sides. Even without a conventional magnetic return path, placing coils on both faces of the rotor leverages the entire available field, mitigating some of the flux leakage that would otherwise occur in a single-sided configuration.

3.5 Finite element analysis (FEA) simulations

Before proceeding to the physical realization of the PCB-based axial flux BLDC motor, it is essential to evaluate and refine the proposed design through comprehensive simulation studies. FEA offers a detailed, physics-based assessment of the machine's electromagnetic behavior under various operating conditions. By employing specialized FEA software tools such as JMAG, the complex interactions between the rotor's magnetic field, the stator winding configuration, and the resulting torque is accurately modeled.

3.5.1 Airgap flux density

To accurately predict the airgap flux density in the axial flux PCB motor, a 3D Finite Element Method (FEM) simulation is employed. One of the key considerations in 3D FEM analysis is the selection of an appropriate mesh size, as the level of mesh refinement can greatly influence both the accuracy of the results and the required computational resources.

The process begins with a relatively coarse mesh, which involves fewer elements and nodes. While this initial setup provides a rapid approximation of the motor's electromagnetic field, the coarse discretization may lack the resolution needed to capture fine variations in flux density, particularly around the stator-rotor interface. As the mesh is refined, by increasing the number of elements and improving element quality, the simulation's fidelity improves.

A finer mesh better represents the complex geometry of the rotor magnets, stator windings, and the thin airgap region, leading to more accurate calculations of the local flux densities. Each refinement step is guided by a balance between accuracy and computation time. While finer meshes reduce numerical discretization errors and stabilize the flux density results, they also increase the number of degrees of freedom and, consequently, the simulation's computational cost. To find a suitable mesh size, a series of simulations are performed, starting from a coarse mesh and progressively refining it until the computed airgap flux density values converge within an acceptable tolerance.

During this convergence study, metrics such as the average airgap flux density and its harmonic content are monitored. When successive refinements produce negligible changes in these metrics, it indicates that the solution has reached mesh convergence. At this point, the chosen mesh is 0.3mm and it provides a stable and reliable estimate of the airgap flux distribution without incurring prohibitively long computation times. By selecting a mesh density that strikes a balance between computational efficiency and result fidelity, the simulation can effectively capture the underlying physics of the axial flux PCB motor's electromagnetic environment. The mesh quality assessment is shown in Fig. 3.6, which provides a distribution of element quality that indicates most elements meet acceptable standards. Meanwhile, Fig. 3.7 shows the final meshing of the proposed PCB motor design.

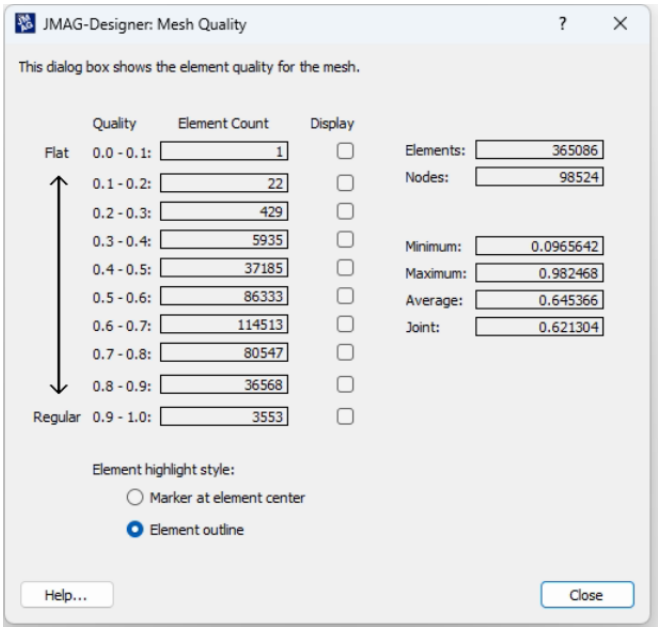

Fig. 3.6 Elements quality for the mesh

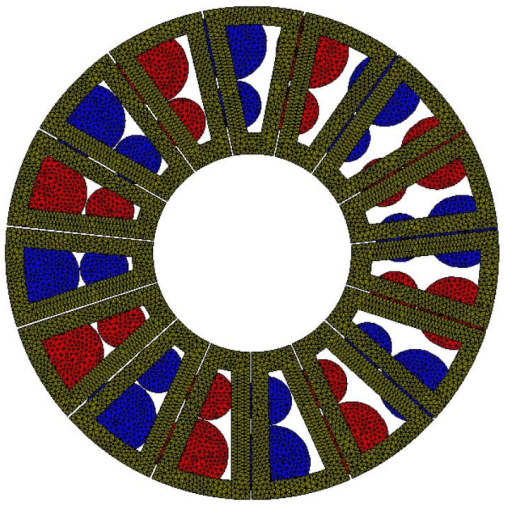

Fig. 3.7 Mesh view of the proposed PCB motor

The desired average airgap flux density for the proposed axial flux PCB motor was set to 0.6 T. As shown in the waveform of the airgap flux density in Fig. 3.8, the simulation results closely match this target value, demonstrating that the chosen magnet configuration, stator design, and mesh resolution are appropriate. Following the successful verification of the flux density magnitude, it is equally important to understand how the flux is spatially distributed within the machine. The flux distribution contour plot in Fig. 3.9 visually represents the magnetic intensity across the rotor and stator domains.

This visualization helps to verify that the magnets and PCB stator coils interact as intended, with flux lines passing uniformly through the airgap. Identifying regions of peak flux density and verifying that no areas exhibit anomalously low or distorted fields is crucial for validating the electromagnetic design and ensuring that the intended flux paths are maintained.

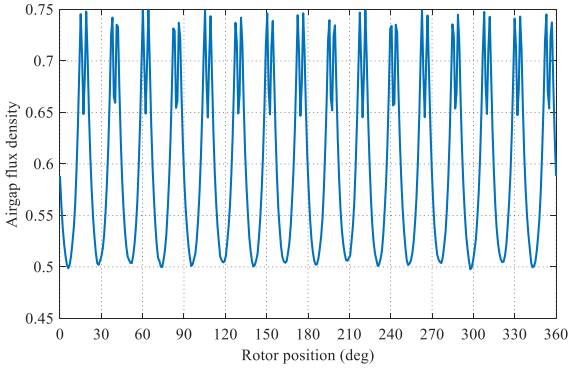

Fig. 3.8 Airgap flux density waveform

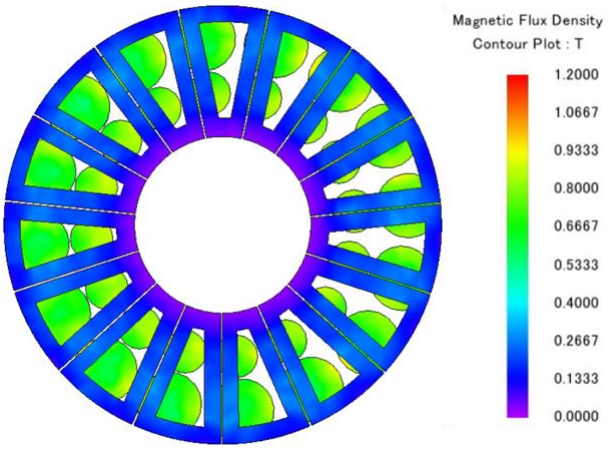

Fig. 3.9 Flux distribution of PCB motor

3.5.2 Back emf

Back-EMF is a critical parameter in motor design, as it directly relates to how the machine's generated voltage changes with rotor speed and magnetic field interaction. To evaluate this behavior, back-EMF waveforms at both the motor's rated speed (30,000 rpm) and half the rated speed (15,000 rpm) are examined. The amplitude of the back-EMF is largely proportional to the rotor speed. At the full rated speed of 30,000 rpm, the peak voltage is almost 50% higher compared to the half-rated speed condition (15,000 rpm) as shown in Fig. 10 and Fig. 11 respectively. This outcome aligns with the fundamental principle that back-EMF in a PM BLDC machine scales with the rotor's angular velocity and the magnetic flux linkage. The presented back-EMF waveforms appear sinusoidal and balanced among the three phases (A, B, and C).

A smooth and sinusoidal waveform is desirable, as it reduces torque ripple and facilitates more efficient electronic commutation. The uniformity across phases indicates that the stator coil distribution, pole combination, and rotor magnet arrangement are effective, resulting in symmetrical flux linkage as the rotor rotates. As the coils are connected in parallel, the voltage across each path is identical. In this multi-layer PCB stator, although each layer experiences the same flux linkage and thus generates an equivalent induced voltage, connecting the layers in parallel ensures that the back-EMF across the combined set of layers is not increased. Instead, the total available current capacity of the windings is enhanced. Essentially, while adding more layers in parallel allows higher current flow and

improves torque capability, it does not alter the induce phase voltage (back-EMF) level.

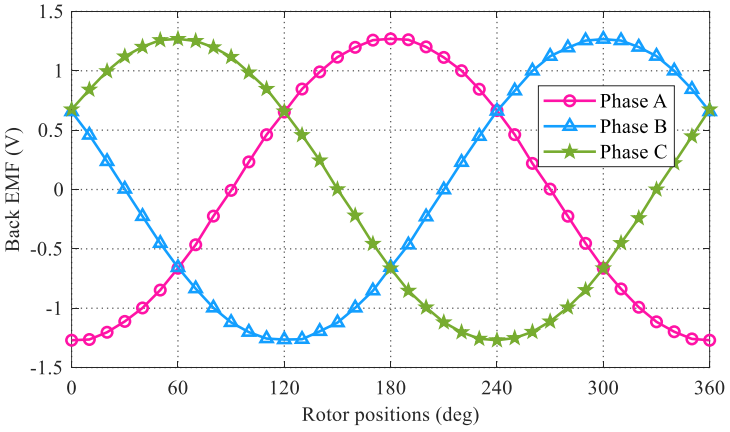

Fig. 3.10 Back EMF waveform at full rated speed of 30,000 rpm

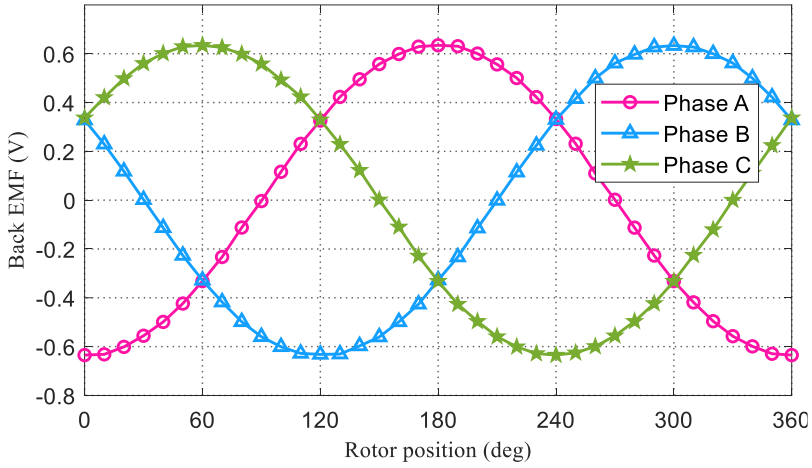

Fig. 3.11 Back EMF waveform at half rated speed of 15,000 rpm

3.5.3 Thermal considerations

The maximum allowable current density in the windings is found with the help of a thermal model. As the motor's intended application is for electrical propulsion, the cooling effect created by the propeller's airflow is considered. Therefore, the model includes a non-isothermal fluid dynamics simulation, which aims to accurately model the temperature increase in the windings at different current density and air velocity values.

The fluid dynamics model consists of a circular sector corresponding to a single slot of the stator and the volume of air around it. The PCB stator is constructed from alternating layers of insulating material ($\lambda_{FR4} = 0.3\ \mathrm{W/(m \cdot K)}$) and copper, with an additional layer of solder mask ($\lambda_{SM} = 0.3\ \mathrm{W/(m \cdot K)}$) covering the outer copper layers.

The losses in the windings $P_{Cu}\ (\mathrm{W})$ are modelled as volumetric heat generation in the copper bodies, which is calculated based on current density and resistivity:

$$P_{Cu} = j^2 \cdot \rho_{Cu} \tag{3.5}$$

The airflow created by the propeller is represented as a velocity inlet, with the fluid modelled as laminar and incompressible to ensure a fast simulation time. The mesh for the entire model consists of approximately 10^6 elements. The temperature distribution in the copper layers is shown in Fig. 3.12. The topology of the motor results in a large amount of cooling for the upper stator, while the lower one only receives incidental airflow created by a low-pressure zone near the edge of the PCB. Therefore, a large temperature difference between the stators is created and the hotspot develops in the lowest copper layer of the bottom stator.

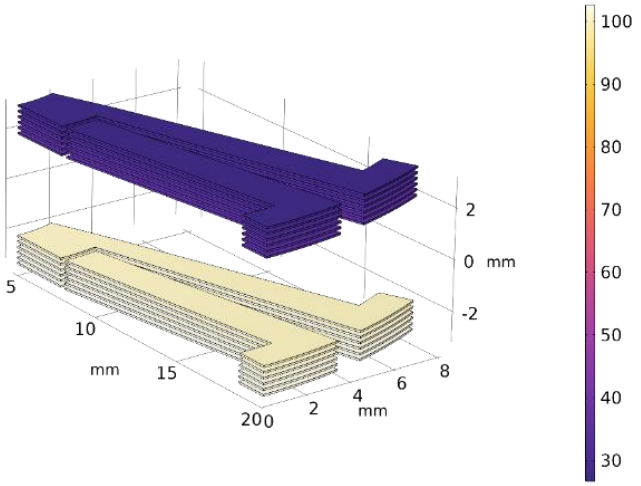

Fig. 3.12 Temperature distribution in the copper layers

Fig. 3.13 presents the hotspot temperatures at various current density and inlet velocity values. The results of the thermal model show that the cooling effect for the bottom stator is highly dependent on inlet velocity, even though the interaction between the airflow and bottom stator is limited. For the purposes of this paper, an inlet velocity value of 5 m/s is considered, meaning that a current density value of 20 $\mathrm{A/mm^2}$ can be used without exceeding a hotspot temperature value of 100 °C.

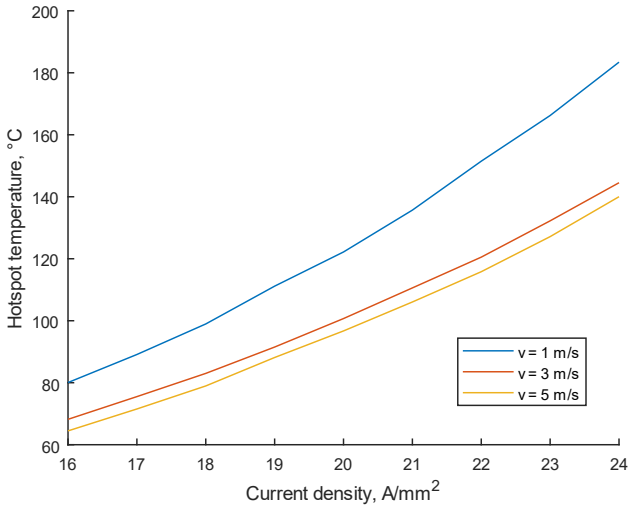

Fig. 3.13 Hotspot temperatures at different inlet velocity values and an ambient temperature of 20°C

3.5.4 Torque vs current characteristics

The analysis now focuses on the electromagnetic output performance of the proposed axial flux PCB motor, particularly examining its torque and current waveforms. The instantaneous torque over one mechanical revolution and the corresponding phase currents under a given operating speed of 30,000 rpm are shown in Fig. 3.14 and Fig. 3.15 respectively. The torque waveform shows that the machine produces a relatively steady torque output around the desired operating point, with slight variations and ripple rate of 16.08%.

The current waveform, depicted for the machine's three phases, shows that the current levels fluctuate as a function of rotor position. In this design, a single PCB stator with six copper layers in parallel is employed per phase. Since all layers are electrically connected in parallel, the total current shown in the figure represents the cumulative current through all six layers. Given a current density target of approximately 16 A/mm², the resulting phase current of

around 10 A is effectively divided among the six parallel layers, leading to 1.66 A per layer. This distribution ensures that no single layer exceeds the permissible current density, maintaining the thermal and reliability constraints of the design.

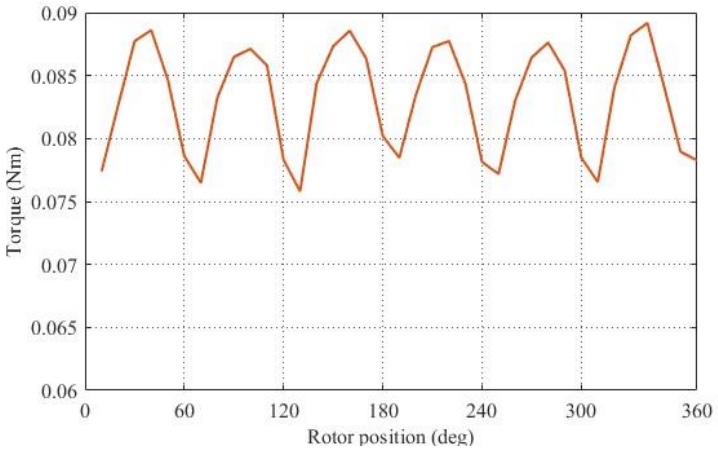

Fig. 3.14 Instantaneous torque waveform of proposed PCB motor

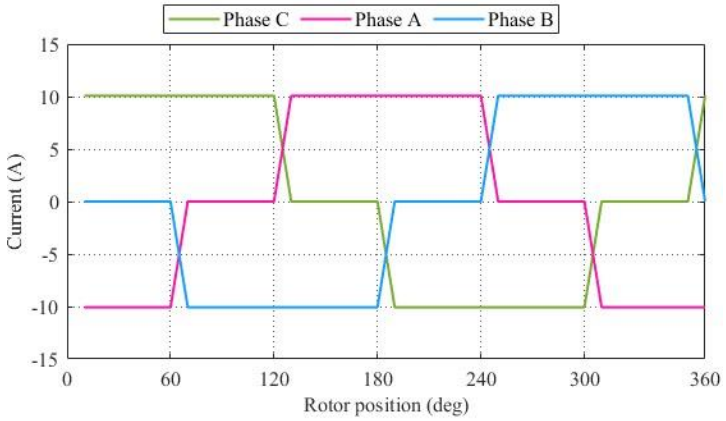

Fig. 3.15 Three phase current waveform of single PCB stator

3.6 Assembly and prototyping

The assembly of the proposed axial flux PCB motor involves integrating all mechanical and electromagnetic components into a stable, functional structure. The design prioritizes simplicity, accuracy, and manufacturability, ensuring that each element fits together cohesively while maintaining precise alignment for optimal electromagnetic performance. As shown in the exploded view in Fig. 3.16, the motor's core components are enclosed

between two mounting supports. These supports serve several purposes discussed below:

Bearing housings:

Each support features a machined recess to hold a standard ball bearing. The bearings provide a low-friction rotational interface for the rotor shaft, ensuring smooth and stable operation. By positioning bearings on both sides, the assembly balances axial forces and reduces wobble, maintaining a uniform airgap between the rotor and stators.

PCB stator placement:

The PCB stators, each comprising six copper layers, are positioned within grooves machined into the mounting supports. This secure nesting prevents lateral movement, maintains consistent alignment with the rotor, and ensures the correct axial positioning to achieve the desired thin airgap. Tight tolerances on the stator mounting surfaces help preserve the geometry established during the design and simulation phases.

Shaft alignment and assembly:

A central shaft passes through the bearings and supports, providing the rotational axis for the rotor assembly. Ensuring that the shaft is straight and precisely fitted into the bearings is critical for minimizing runout and maintaining uniform airgap spacing as the rotor spins.

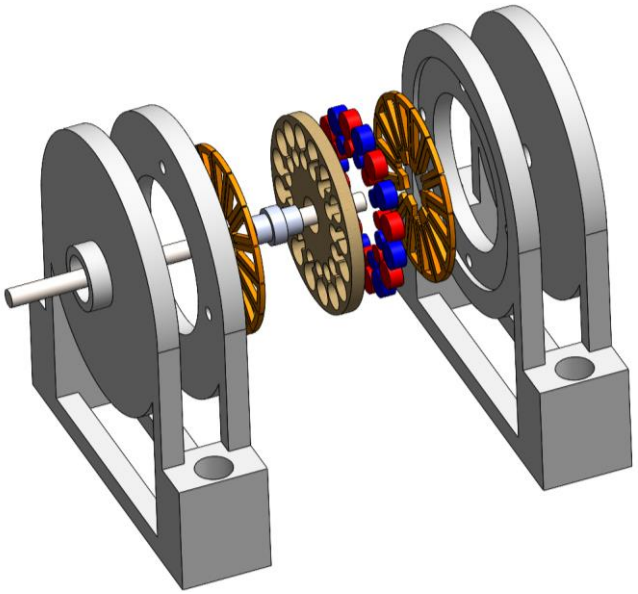

Fig. 3.16 Exploded view of the of the prototype and assembly with supports

The rotor is formed using a 3 mm-thick PCB sheet. Precision drilling operations create apertures sized to accommodate two distinct sets of magnets, chosen to emulate the flux distribution of wedge magnets while using readily available, lower-cost disc magnets. Each magnet is carefully inserted into its designated hole in the PCB, ensuring a tight fit and secure placement. The magnets are arranged according to the selected pole configuration (e.g., the 15/16 combination) to achieve the required flux pattern. By using a PCB rotor, the magnet placement process becomes more repeatable and less labor-intensive than traditional assembly methods.

The PCB's inherent dimensional stability and flatness contribute to consistent magnet-to-stator spacing, further enhancing machine performance. The PCB stators are fabricated using a multi-layer manufacturing process, stacking six copper layers to increase current capacity without altering the number of turns. Multiple copper layers are printed and etched to form the single-turn wave winding configuration.

This process ensures precise conductor geometry, adherence to design clearances, and consistent copper thickness. Vias interconnect the layers, ensuring that each winding path is continuous in the vertical direction. This technique enables current to flow uniformly among the parallel layers, maintaining the desired current density and mitigating localized heating. The PCB stator configuration for the proposed machine is shown in Fig. 3.17, while the PCB rotor, complete with carefully positioned magnets, is presented in Fig. 3.18.

Fig. 3.17 Axial flux PCB stator comprising six layers

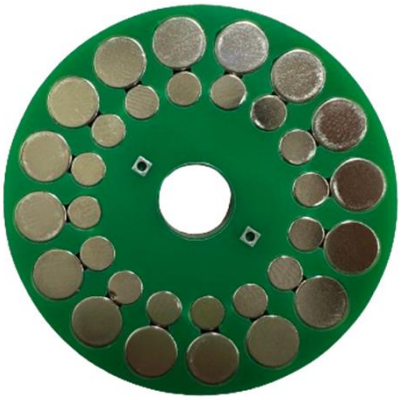

Fig. 3.18 Axial flux PCB rotor

3.7 Experimental validation

To validate the simulated results and assess the practical performance of the proposed axial flux PCB motor, a dedicated experimental setup was arranged. The prototype was mounted securely and coupled to a prime mover, which is an external motor serving as a controlled speed source. This arrangement allowed for precise control over the rotor speed while the stator windings were left open-circuited to measure the induced back-EMF. torque sensor, placed in-line between the prime mover and the test motor, provided real-time measurements of shaft speed. The three-phase back-EMF was recorded using an oscilloscope connected directly to the stator terminals. Adjustable speed control of the prime mover enabled testing at different operating points, such as 2,500 rpm and 4,000 rpm, ensuring a wide operating range for the validation process. Fig. 3.19 shows the complete experimental setup for the proposed axial flux PCB motor.

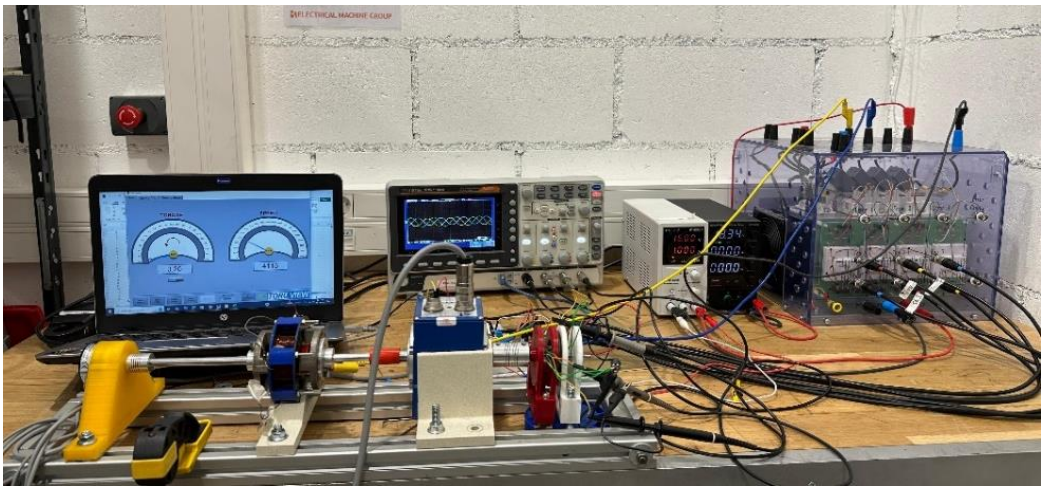

Fig. 3.19 Experimental setup of the proposed axial flux PCB motor

The measured back-EMF waveforms were analyzed and compared against the simulated predictions. At a test speed of 2,500 rpm, the difference between simulated and measured back-EMF values was observed to be in the range of approximately 10–11%, as shown in Fig. 3.20. When the speed was increased to 4,000 rpm, the discrepancy rose slightly to around 12%, as presented in Fig. 3.21. These variations are within a reasonable margin, especially considering the idealized assumptions made during the simulation phase. Several factors can contribute to these differences, e.g. variations in PCB fabrication, magnet placement, and mechanical assembly can introduce slight geometric deviations. Even small alignment errors or differences in airgap thickness can affect the flux linkage and thus the induced voltage. The oscilloscope and sensors introduce their own measurement uncertainties. Additionally, any vibration, shaft misalignment, or bearing friction in the test setup can influence the observed back EMF to a minor extent.

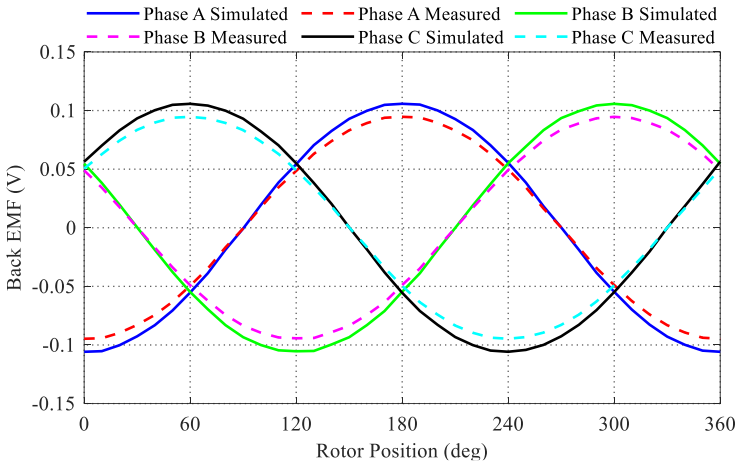

Fig. 3.20 Simulated and measured three phase back EMF at 2500 rpm

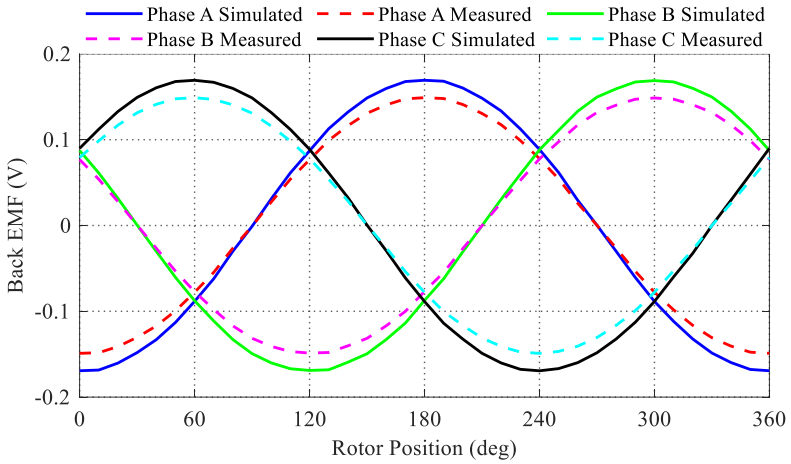

Fig. 3.21 Simulated and measured three phase back EMF at 4000 rpm

The second measurement performed on the prototype aims to approximate the steady-state torque of the motor by indirectly measuring the maximum holding torque. For this, two phases were excited using a variable DC supply. The torque was measured using a lever arm, which was fixed to the rotor shaft on one end and pressed on a scale from the other. By accounting for the length of the lever arm and reading the value from the scale, the static torque of the motor could be effectively calculated. Although this type of measurement does not directly give the working torque of the motor, it can be considered a good alternative. The results of the torque measurements at different excitation values are presented in fig.3.22. The maximum torque achieved on maximum rated current of 10.08 A recorded is approximately 0.0738 Nm. During the testing it was found that increasing the

current above 11 A caused the temperature of the winding to increase excessively as the cooling effect created by the propeller's airflow is not present. The calculated average torque of the motor at the rated current is approximately 0.083 Nm.

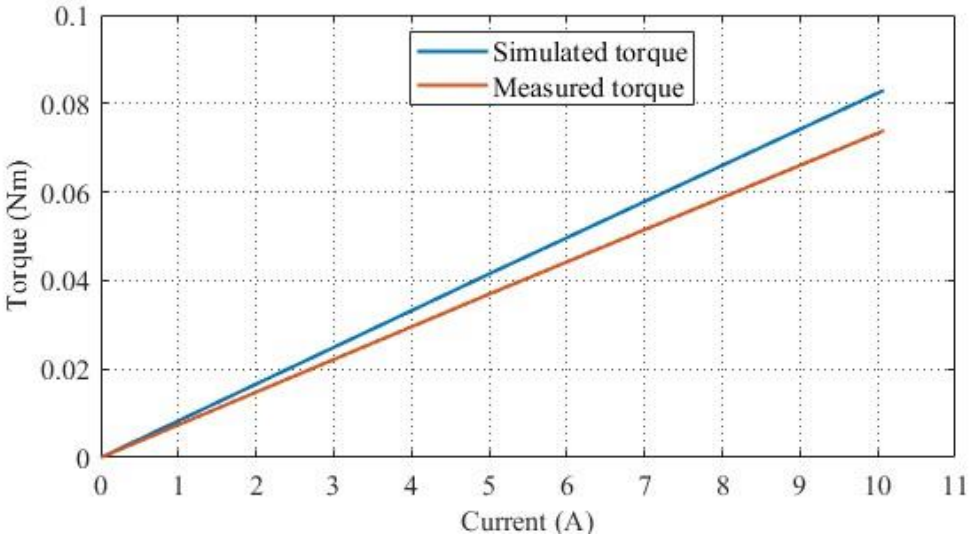

Fig. 3.22 Comparison between simulated and measured torque

3.8 Conclusion

This thesis presented the design, simulation, and experimental validation of a coreless axial flux PCB motor tailored for disposable drone applications. The motor design leveraged rapid manufacturing capabilities through multilayer PCB technology, compact size, and cost-efficient production. A dual-stator configuration was adopted to maximize the utilization of rotor magnetic flux.

The combination of PCB technology with axial flux motor topology provided an effective solution to achieve high power density while maintaining a compact form factor. The stator incorporated six copper layers connected in parallel, which enhanced the current-carrying capacity while maintaining uniform current density and minimal resistive losses. Then the FEA simulations were carried out which ensured that the airgap flux density met the desired target of 0.6T, with mesh convergence studies validating the simulation accuracy and computational efficiency.

Back-EMF waveforms at full-rated (30,000 rpm) and half-rated speeds (15,000 rpm) were analyzed, revealing sinusoidal, well-balanced phase voltages, which are critical for smooth motor operation. The torque output demonstrated a relatively stable performance, with slight ripple attributed to mechanical and geometrical factors. The phase current waveform indicated proper distribution of cumulative current across the six PCB layers.

The motor prototype was extensively tested using a dedicated experimental setup, where it was coupled with a prime mover to evaluate back-EMF and torque performance. The measured results validated the simulated predictions, confirming the feasibility and practicality of the proposed design. Also, the assembly process highlighted the advantages of PCB-based manufacturing, such as precision, scalability, and repeatability. The use of multi-layer stators and cost-effective disc magnets reduced complexity and production costs, making the motor suitable for disposable drone applications.

SUMMARY

Efficient electrical machines are essential for advancements in transportation, renewable energy, and industrial automation. Drones have revolutionized industries such as logistics, agriculture, surveillance, and disaster response, relying heavily on motors for their performance, efficiency, and versatility. To meet these needs, coreless motors have emerged as an ideal solution for drones due to their lightweight design, high torque density, and ease of manufacturing.

This thesis presents the development, simulation, and testing of a coreless axial flux PCB motor designed for disposable drones. Utilizing multilayer PCB technology, the motor achieves rapid, cost-effective production, a compact size, and high-power density. A dual-stator configuration was implemented to maximize rotor magnetic flux. The stator features six parallel-connected copper layers, which enhance current capacity and ensure uniform current distribution with minimal losses.

Finite Element Analysis (FEA) simulations confirmed that the motor reached the target airgap flux density of 0.6T, with mesh studies validating the accuracy and efficiency of the simulations. Back-EMF tests at 30,000 rpm and 15,000 rpm showed smooth, balanced voltages essential for stable motor operation. The torque output remained consistently stable, with only slight ripples due to mechanical and geometric factors. Current distribution across the six PCB layers was even, ensuring reliable performance.

Extensive prototype testing validated the simulation results, demonstrating the design's feasibility and practicality. The assembly process highlighted the advantages of PCB-based manufacturing, including precision, scalability, and repeatability. Additionally, using multilayer stators and cost-effective disc magnets reduced complexity and production costs, making the motor well-suited for disposable drone applications.

KOKKUVÕTE

Tõhusad elektrimasinad on transpordi, taastuvenergia ja tööstusautomaatika edendamiseks hädavajalikud. Droonid on revolutsiooniliselt muutnud selliseid tööstusharusid nagu logistika, põllumajandus, seire ja katastroofidele reageerimine, tuginedes oma jõudluse, tõhususe ja mitmekülgsuse osas suuresti mootoritele. Nende vajaduste rahuldamiseks on südamikuta mootorid oma kerge disaini, suure pöördemomendi tiheduse ja tootmise lihtsuse tõttu kujunenud droonide jaoks ideaalseks lahenduseks.

See doktoritöö tutvustab ühekordselt kasutatavate droonide jaoks mõeldud südamikuta aksiaalse vooga PCB-mootori väljatöötamist, simulatsiooni ja testimist. Kasutades mitmekihilist PCB-tehnoloogiat, mootor saavutab kiire, kulutõhus tootmine, kompaktne suurus, ja suur võimsustihedus. Rootori magnetvoo maksimeerimiseks rakendati kahe staatori konfiguratsiooni. Staatoril on kuus paralleelselt ühendatud vaskkihti, mis suurendavad voolutugevust ja tagavad ühtlase voolujaotuse minimaalsete kadudega.

Lõplike elementide analüüsi (FEA) simulatsioonid kinnitasid, et mootor saavutas sihtmärgiks oleva õhuvoolu tiheduse 0.6T, kusjuures võrgusilma uuringud kinnitasid simulatsioonide täpsust ja tõhusust. Back-EMF testid kiirusel 30 000 p / min ja 15 000 p / min näitasid sujuvaid ja tasakaalustatud pingeid, mis on olulised mootori stabiilseks tööks. Pöördemomendi väljund püsis püsivalt stabiilsena, mehaanilistest ja geomeetrilistest teguritest tingitud vaid kergete pulsatsioonidega. Praegune jaotus kuue PCB kihi vahel oli ühtlane, tagades usaldusväärse jõudluse.

Ulatuslik prototüübi testimine valideeris simulatsiooni tulemused, näidates disaini teostatavust ja praktilisust. Montaažiprotsess tõi esile PCB-põhise tootmise eelised, sealhulgas täpsus, mastaapsus, ja korratavus. Lisaks vähendas mitmekihiliste staatorite ja kulutõhusate ketasmagnetite kasutamine keerukust ja tootmiskulusid, muutes mootori hästi sobivaks ühekordselt kasutatavate droonirakenduste jaoks.

REFERENCES

[1] R. C. Bolam, Y. Vagapov, and A. Anuchin, "A Review of Electrical Motor Topologies for Aircraft Propulsion," in *2020 55th International Universities Power Engineering Conference (UPEC)*, Sep. 2020, pp. 1–6. doi: 10.1109/UPEC49904.2020.9209783.

[2] A. Aabid *et al.*, "Reviews on Design and Development of Unmanned Aerial Vehicle (Drone) for Different Applications".

[3] A. Habib *et al.*, "A systematic review on current research and developments on coreless axial-flux permanent-magnet machines," *IET Electric Power Applications*, vol. 16, no. 10, pp. 1095–1116, 2022, doi: 10.1049/elp2.12218.

[4] D. Lawhorn, P. Han, D. Lewis, Y. Chulaee, and D. M. Ionel, "On the Design of Coreless Permanent Magnet Machines for Electric Aircraft Propulsion," in *2021 IEEE Transportation Electrification Conference & Expo (ITEC)*, Jun. 2021, pp. 278–283. doi: 10.1109/ITEC51675.2021.9490162.

[5] D. Gheorghita, I. Vintu, L. Mirea, and C. Braescu, "Quadcopter control system," in *2015 19th International Conference on System Theory, Control and Computing (ICSTCC)*, Cheile Gradistei, Romania: IEEE, Oct. 2015, pp. 421–426. doi: 10.1109/ICSTCC.2015.7321330.

[6] "Development and Research the Coreless Micro Electric Drive Model of RC Drone | IEEE Conference Publication | IEEE Xplore." Accessed: Dec. 15, 2024. [Online]. Available: https://ieeexplore.ieee.org/abstract/document/10755784

[7] T. Ghanbari, M. Sanati Moghadam, and A. Darabi, "Comparison between coreless and slotless kinds of dual rotor discs hysteresis motors," *IET Electric Power Applications*, vol. 10, no. 2, pp. 133–140, 2016, doi: 10.1049/iet-epa.2015.0188.

[8] "Design aspects, winding arrangements and applications of printed circuit board motors: a comprehensive review - Taqavi - 2020 - IET Electric Power Applications - Wiley Online Library." Accessed: Dec. 15, 2024. [Online]. Available: https://ietresearch.onlinelibrary.wiley.com/doi/full/10.1049/iet-epa.2020.0141

[9] J. F. Gieras and I. A. Gieras, "Performance analysis of a coreless permanent magnet brushless motor," in *Conference Record of the 2002 IEEE Industry Applications Conference. 37th IAS Annual Meeting (Cat. No.02CH37344)*, Oct. 2002, pp. 2477–2482 vol.4. doi: 10.1109/IAS.2002.1042794.

[10] N. Taran, V. Rallabandi, and D. M. Ionel, "WAVED: A Coreless Axial Flux PM Motor for Drive Systems with Constant Power Operation," in *2019 IEEE Transportation Electrification Conference and Expo (ITEC)*, Jun. 2019, pp. 1–6. doi: 10.1109/ITEC.2019.8790489.

[11] C. Soneda, H. Asai, Y. Hatta, T. Shimono, and K. Ohnishi, "Design and Analysis of Core-less Multi-layered Axial Motor," in *2019 IEEE 28th International Symposium on Industrial Electronics (ISIE)*, Jun. 2019, pp. 267–272. doi: 10.1109/ISIE.2019.8781345.

[12] N. S., S. P. Nikam, S. Pal, A. K. Wankhede, and B. G. Fernandes, "Performance Comparison Between PCB-Stator and Laminated-Core-Stator-Based Designs of Axial Flux Permanent Magnet Motors for High-Speed Low-Power Applications," *IEEE Transactions on Industrial Electronics*, vol. 67, no. 7, pp. 5269–5277, Jul. 2020, doi: 10.1109/TIE.2019.2931503.

[13] L. Yang, J. Zhao, X. Liu, A. Haddad, J. Liang, and H. Hu, "Comparative Study of Three Different Radial Flux Ironless BLDC Motors," *IEEE Access*, vol. 6, pp. 64970–64980, 2018, doi: 10.1109/ACCESS.2018.2878267.

[14] N. S., S. P. Nikam, S. Singh, S. Pal, A. K. Wankhede, and B. G. Fernandes, "High-Speed Coreless Axial-Flux Permanent-Magnet Motor With Printed Circuit Board Winding," *IEEE Transactions on Industry Applications*, vol. 55, no. 2, pp. 1954–1962, Mar. 2019, doi: 10.1109/TIA.2018.2872155.

[15] M. Liu, K. W. Chan, J. Hu, Q. Lin, J. Liu, and W. Xu, "Design and Realization of a

Coreless and Magnetless Electric Motor Using Magnetic Resonant Coupling Technology," *IEEE Transactions on Energy Conversion*, vol. 34, no. 3, pp. 1200–1212, Sep. 2019, doi: 10.1109/TEC.2019.2894865.
[16] N. Taran, V. Rallabandi, G. Heins, and D. M. Ionel, "Coreless and Conventional Axial Flux Permanent Magnet Motors for Solar Cars," *IEEE Transactions on Industry Applications*, vol. 54, no. 6, pp. 5907–5917, Nov. 2018, doi: 10.1109/TIA.2018.2855123.
[17] B. Liu, R. Badcock, H. Shu, L. Tan, and J. Fang, "Electromagnetic Characteristic Analysis and Optimization Design of a Novel HTS Coreless Induction Motor For High-Speed Operation," *IEEE Transactions on Applied Superconductivity*, vol. 28, no. 4, pp. 1–5, Jun. 2018, doi: 10.1109/TASC.2018.2793666.
[18] V. Rallabandi, N. Taran, D. M. Ionel, and J. F. Eastham, "On the feasibility of carbon nanotube windings for electrical machines — Case study for a coreless axial flux motor," in *2016 IEEE Energy Conversion Congress and Exposition (ECCE)*, Sep. 2016, pp. 1–7. doi: 10.1109/ECCE.2016.7855306.
[19] F. Marcolini, G. De Donato, F. G. Capponi, and F. Caricchi, "A Comparative Study of Stator Winding Technologies for Coreless Axial Flux Permanent Magnet Machines," in *2024 International Conference on Electrical Machines (ICEM)*, Sep. 2024, pp. 1–7. doi: 10.1109/ICEM60801.2024.10700133.
[20] C. Wang, J. Han, Z. Zhang, Y. Hua, and H. Gao, "Design and Optimization Analysis of Coreless Stator Axial-Flux Permanent Magnet In-Wheel Motor for Unmanned Ground Vehicle," *IEEE Transactions on Transportation Electrification*, vol. 8, no. 1, pp. 1053–1062, Mar. 2022, doi: 10.1109/TTE.2021.3093931.
[21] Y. Liu, Z. Zhang, C. Wang, W. Geng, and T. Yang, "Design and Analysis of Oil-Immersed Cooling Stator With Nonoverlapping Concentrated Winding for High-Power Ironless Stator Axial-Flux Permanent Magnet Machines," *IEEE Transactions on Industrial Electronics*, vol. 68, no. 4, pp. 2876–2886, Apr. 2021, doi: 10.1109/TIE.2020.2978694.
[22] D. J. Patterson, J. L. Colton, B. Mularcik, B. J. Kennedy, S. Camilleri, and R. Rohoza, "A comparison of radial and axial flux structures in electrical machines," in *2009 IEEE International Electric Machines and Drives Conference*, May 2009, pp. 1029–1035. doi: 10.1109/IEMDC.2009.5075331.
[23] S. Amin, S. Khan, and S. S. Hussain Bukhari, "A Comprehensive Review on Axial Flux Machines and Its Applications," in *2019 2nd International Conference on Computing, Mathematics and Engineering Technologies (iCoMET)*, Jan. 2019, pp. 1–7. doi: 10.1109/ICOMET.2019.8673422.
[24] A. Mukminin and M. Tadjuddin, "Rancang Bangun Generator Linier Magnet Permanen".